Ann. Geophys. Discuss., https://doi.org/10.5194/angeo-2018-13
Manuscript under review for journal Ann. Geophys.
Discussion started: 13 February 2018

Annales Geophysicae
Discussions

On the convection of ionospheric density features

John D. de Boer[1], Jean-Marc A. Noël[1], and Jean-Pierre St.-Maurice[2]

[1]Royal Military College, P.O. Box 17000, Kingston, ON, Canada
[2]Institute of Space and Atmospheric Studies, University of Saskatchewan, Saskatoon, SK, Canada

Correspondence: John D. de Boer (john.deBoer@rmc.ca)

Abstract. We investigate whether the boundaries of an ionospheric region of different density than its surroundings will drift relative to the background $\boldsymbol{E} \times \boldsymbol{B}$ drift and, if so, how the drift depends on the degree of density enhancement and the altitude. We find analytic solutions for discrete circular features in a 2-D magnetised plasma. The relative drift is proportional to the density difference, which suggests that where density gradients occur they should tend to steepen on one side of a patch while they are weakened on the other. This may have relevance to the morphology of polar ionospheric patches and auroral arcs, since the result is scale-invariant. There is also an altitude dependence which enters through the ion-neutral collision frequency. We discuss how the 2-D analytic result can be applied to the real ionosphere.

1 Introduction

We are investigating the fundamental transport properties of cold, magnetised plasmas. There appears to be a characteristic property of $\boldsymbol{E} \times \boldsymbol{B}$ drift which has not been previously elucidated and which we examine here. The expression for this drift field $\mathbf{v}_\mathrm{a}$ (subscript *a* for *ambipolar*) is

$$\mathbf{v}_\mathrm{a} = \frac{\boldsymbol{E} \times \boldsymbol{B}}{B^2} \tag{1}$$

which does not involve either mass or number density, or indeed *any* of the intrinsic properties of the plasma. The phenomenon of ambipolar drift can be understood either from the trochoidal trajectory of individual particles, or from the Lorenz transformation, which shows that for a magnetised plasma there is a "preferred" frame of reference (this $\mathbf{v}_\mathrm{a}$) in which the perpendicular electric field $\boldsymbol{E}_\perp$ vanishes.

The $\boldsymbol{E} \times \boldsymbol{B}$ drift is independent of the plasma properties – *for a given* $\boldsymbol{E}$. However we may ask how the electric field will be arranged in and around a density feature. We show that $\boldsymbol{E}$ can and will likely be structured in such a way that $\boldsymbol{E} \times \boldsymbol{B}$ drift *does* depend inversely on the plasma mass density in most situations. The conditions under which our initial assumptions prevail in the ionosphere and magnetosphere will also be discussed.

The analysis we present entails certain simplifying assumptions, the chief of which is uniformity along magnetic field lines, also called a 2-D plasma. More precisely, it means that the location of plasma *along* a field line is considered unimportant,

Ann. Geophys. Discuss., https://doi.org/10.5194/angeo-2018-13
Manuscript under review for journal Ann. Geophys.
Discussion started: 13 February 2018

Annales Geophysicae Discussions
Open Access

so that we need to consider only height-integrated (or field-line averaged) plasma properties. This assumption is clearly a significant one in the ionosphere, especially in the E-region. However the high parallel conductivity at all altitudes causes magnetic field lines to have a consistent electric potential, which forces the $\boldsymbol{E}\times\boldsymbol{B}$ drift to be mapped along the entire flux tube (propagated at the Alfvén speed). And we can show that on *closed* field lines our results are still applicable to an ionospheric situation. We believe that numerical modelling with realistic field-line gradients will also substantiate this analysis.

We discuss electric field rearrangements, denoted $\delta\boldsymbol{E}_\perp$, which require finite time to propagate through the 2-D domain perpendicular to $\boldsymbol{B}$. However the low-frequency (DC) limit for *perpendicular* EM propagation in the ionosphere is also the Alfvén speed, $\mathrm{v_A}$, as shown e.g. by Baumjohann and Treumann (1996, Eq. 9.142). Typical ambipolar drifts are *much* slower, so one can assume that $\delta\boldsymbol{E}_\perp$ propagates effectively instantaneously.

We call the electric field far from the density features we consider the "background" electric field, $\boldsymbol{E}_0$. And as we shall see below, the background field can only be uniform if the background density is as well.

If we were to address *collisionless* plasma, i.e. with no significant ion-neutral collisions, there is a train of argument we can take to show how the electric field becomes structured merely by propagating through density features. The result one obtains is the same as we obtain below, if we then look at the limit of collision frequency approaching zero; the time scale is finite and dependent on propagation, not collisions. However this case entails as much work as this already lengthy article, and will hopefully be the subject of a follow-on paper. The results below are more than adequate for any *ionospheric* conditions.

In this treatment, we assume that there are no field-aligned currents (FACs) within our domain of interest. Instead the electric field, and associated plasma drift, occur because of driving forces *outside* our domain. In a region of *open* field lines, or where the plasma is being forced *locally* by the neutral dynamo, the drift speed could remain independent of local density, e.g. the polar-cap potential field is "mapped" there more or less directly from the interplanetary electric field. But it still creates an electric field on *closed* field lines in the polar regions. The scenarios we study are an idealisation of conditions in the polar oval, but as long as there is an electric field in the frame of the neutrals our results apply in some measure.

We shall examine a circular plasma density feature, either an enhancement or a depletion. For ease of reference we use the word "patch" in this paper, but with that term we don't mean *only* features that are two times or greater in density than the background, which is its conventional definition (e.g. Carlson, 2012).

Let the density of the patch be n times the background density. Thus a depletion is a density feature with $0<n<1$. For ease of later notation, we find it useful to define another dimensionless quantity:

$$\eta = \frac{n-1}{n+1} \tag{2}$$

Thus η serves as an alternate parameterisation of relative density such that $-1<\eta<1$, the bounds corresponding to an extreme depletion ($\eta\to-1$ as $n\to 0$) or an extremely dense patch ($\eta\to 1$ as $n\to\infty$).

1.1 Boundary condition on moving interface

In studying a scenario with varying density and drift speed, we must maintain conservation of particle number by species. This leads to a constraint on the speed at which the *boundary* drifts.

Ann. Geophys. Discuss., https://doi.org/10.5194/angeo-2018-13
Manuscript under review for journal Ann. Geophys.
Discussion started: 13 February 2018

Annales Geophysicae Discussions Open Access EGU

Let $\hat{\boldsymbol{n}}$ be an outward normal, and let ρ_s be the density of species s. If we call the drift of the boundary $\mathbf{v}_\mathrm{b}$ then conservation of particle number requires that at the interface, for each species,

$$\rho_s \hat{\boldsymbol{n}} \cdot (\mathbf{v}_s - \mathbf{v}_\mathrm{b})\Big|_\mathrm{ext} = \rho_s \hat{\boldsymbol{n}} \cdot (\mathbf{v}_s - \mathbf{v}_\mathrm{b})\Big|_\mathrm{int} \tag{3}$$

which we can rearrange to get

$$\hat{\boldsymbol{n}} \cdot \mathbf{v}_\mathrm{b} = \frac{\hat{\boldsymbol{n}} \cdot (n\mathbf{v}_\mathrm{s,int} - \mathbf{v}_\mathrm{s,ext})}{(n-1)} \tag{4}$$

Also, the component of $\mathbf{v}_\mathrm{b}$ tangential to the boundary is arbitrary. So if we obtain a result like Eq. (4) where the bracketed expression on the RHS has no angular dependence, then we can drop $\hat{\boldsymbol{n}}\cdot$ from both sides of the last equation and choose the vector $\mathbf{v}_\mathrm{b}$ to be $(n\mathbf{v}_\mathrm{s,int} - \mathbf{v}_\mathrm{s,ext})/(n-1)$.

There are objections that could be raised to studying sharp boundaries, but we address those challenges in the discussion.

1.2 Validation of 2-D assumption

Let us consider a 2-D plasma with collisions with a neutral gas, like the E-region but isolated from any parallel connections with a higher, collisionless region. It is uniform in the parallel direction, but we shall relate it to a realistic scenario in the discussion. There is a background electric field in the +y direction. The Pedersen and Hall currents will be assumed to be driven by – and to close with – parallel currents far off in the ±y directions.

The FACs have their origin in plasma drifts in the magnetosphere or, in the case of open field lines, in the solar wind. FACs will create or adjust the ionospheric electric field whenever the ionospheric drift is not coherent with the magnetospheric drift: that is, the electric potential is mapped along field lines.

If E-region conductivity features begin to structure $\boldsymbol{E}_\perp$, then initially the F-region will create FACs that reduce the trend. However in App. B we show that the F-region's drift kinetic energy would be absorbed by the E-region in a time on the order of a second or less, leading the F-region to adopt the E-region's $\boldsymbol{E}_\perp$ structure also.

Then, once the whole height of the ionosphere has developed a structured $\boldsymbol{E}_\perp$, the magnetosphere's much greater drift kinetic energy reserve will continue to feed FACs structured in such a way as to restore the ionosphere's drift to the pattern of the magnetosphere's drift.

However, the magnetosphere is far enough from the ionosphere that it cannot provide FACs immediately, once the drift kinetic energy of the F-region has been used up by E-region conductivity. The time for an Alfvén wave to travel to the magnetic equator and back is of order 3 to 5 minutes. And there is only a finite energy available even there. Therefore it is reasonable to consider that most of the auroral ionosphere is typically in a condition where the electric field re-arrangements necessary for the E-region to be in steady state ($\nabla \cdot \boldsymbol{J} = 0$) have been more or less mapped up throughout the F-region as well. (And the E-region would ultimately impose its electric-field structuring upwards onto the remainder of any *closed* field line, given sufficient time.) Moreover, the E-region's conductivity structure will generate $\boldsymbol{E}_\perp$ structure within the time scales of the ion-neutral collision frequency ν_in and of the perpendicular EM propagation, which is also at the Alfvén speed.

Therefore we feel confident in proceeding with an analysis that excludes FACs within the domain of interest, and in which the electric field in the E-region is determined only by the "background" $\boldsymbol{E}_0$ and by E-region conductivity.

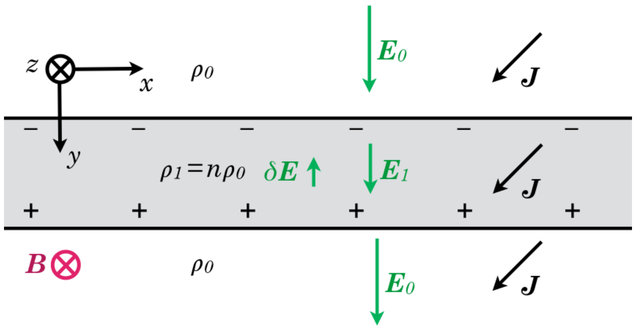

Figure 1. A slab of denser plasma extending perpendicular to the background electric field $\boldsymbol{E}_0$ and extending parallel to $\boldsymbol{B}$ (e.g. between two L-shells). In order for the Pedersen current across the boundaries to be conserved, $\boldsymbol{E}_1$ within the slab will be lower than $\boldsymbol{E}_0$ outside.

1.3 E-region steady state without local FAC

In a uniform 2-D plasma the current density is

$$\boldsymbol{J} = [\sigma]\boldsymbol{E} = \begin{bmatrix} \sigma_\mathrm{P} & -\sigma_\mathrm{H} \\ \sigma_\mathrm{H} & \sigma_\mathrm{P} \end{bmatrix} \boldsymbol{E} \tag{5}$$

where σ_P and σ_H are the Pedersen and Hall conductivities. (We use the letter σ elsewhere for a surface-charge density, so to avoid confusion we write the conductivity matrix as $[\sigma]$.) The components are equal to

$$\sigma_\mathrm{P} = \sum_s \frac{q_s n_s \kappa_s}{B(1+\kappa_s^2)} \tag{6}$$

$$\sigma_\mathrm{H} = \sum_s \frac{q_s n_s}{B(1+\kappa_s^2)} \tag{7}$$

where the sum is over all charged species; q_s, n_s and κ_s are the charge, number density and magnetisation ratio of the species s. The latter is defined as $\kappa_s = \omega_s/\nu_s$, where ω_s is the cyclotron frequency of the species and ν_s is its momentum transfer collision frequency with the neutrals. (We consider both ω_e and κ_e to be negative.)

We denote quantities within the enhancement with a prime. If the patch is a factor n times the number density of the background, assuming similar composition, then $[\sigma]' = n[\sigma]$.

2 A "slab" feature in the E-region

Let us first consider a slab geometry. Assume there is a curtain of plasma as in Fig. 1 with different density than its surroundings. (By *slab* we mean something like different L shells, not *horizontal* strata unless we were at the equator.) We assume Cartesian geometry with $\boldsymbol{B} = B\hat{\boldsymbol{z}}$.

If $\boldsymbol{E}$ were uniform, the higher conductivity inside the slab would build up charge on one boundary and deplete it on the other, creating a $\delta\boldsymbol{E}$ oriented towards $-\hat{\boldsymbol{y}}$ and reducing E within the slab. In steady state, $\delta\boldsymbol{E}$ will be the value that restores $\nabla\cdot\boldsymbol{J}_\perp = 0$.

We can see by inspection that $E' = E_0 + \delta E$ must be inversely proportional to the density ratio n, since the Pedersen current density has to be equal on both sides of the boundary. Provided ν_{in} is constant, the Hall current density remains uniform as well, since the product $E'\sigma'_{\text{H}}$ is concomitantly fixed. The Pedersen component of ion drift is in the $+$y direction, faster outside the layer than within it. This means that ions are piling up on the incoming side of the layer and being peeled away on the other. The net result is that the boundary between the more and less dense regions does *not* move, and that the *ions* within the slab are transient while the electrons remain in it.

3 A circular, E-region patch

Suppose next that there is a circular patch of higher density, as suggested in Fig. 2. The electric field strength E must be lower inside the patch, or else charge would continually build up at the boundary. In fact in steady state there must be a net charge on the interface in order for E to be lower inside. By inspection or simple argument we can see that it will have a cylindrical dipole arrangement.

This problem has been solved already by Hysell and Drexler (2006) using complex analysis, and they have even obtained the solution for a more general elliptical problem using a conformal mapping. Up to Eq. (27) we provide an alternate derivation of the same result. Our method for the circular patch is somewhat less abstract, and perhaps simpler, because it does not use the double shell required for their elliptical result.

The cylindrical (or 2-D) dipole has a distinct character from the spherical dipole that is more familiar in space physics contexts. Using cylindrical polar coordinates ρ and θ, the components of a 2-D dipole aligned with the x axis are (Mallinson, 1981, Eq. 8)

$$a_\rho = \frac{2\mu}{\rho^2}\cos\theta;\ a_\theta = \frac{2\mu}{\rho^2}\sin\theta \tag{8}$$

where μ is a constant and $\boldsymbol{a} = (a_\rho, a_\theta)$ represents the dipole field. Both the field lines and equipotential surfaces of a 2-D dipole are circular. So the disturbed velocity field is also a dipole rotated by 90° as seen in Fig. 3. In App. A we provide a Cartesian expression for the dipole and details of the algebraic steps.

In Figs. 2 and 3 the dipole is aligned with the y axis, and the net charge along the circular boundary has the form $\sigma = \sigma_0\sin\theta$; the sense of θ is shown in Fig. 2. Let $\boldsymbol{E}_{\text{dip}}$ be a vector oriented parallel to the charge dipole and representing its maximum strength; then $\sigma_0 = 2\varepsilon_0 E_{\text{dip}}$. The electric field in and around the patch has the form

$$\boldsymbol{E}_{\text{int}} = \boldsymbol{E}_0 - \boldsymbol{E}_{\text{dip}} \tag{9}$$

$$\boldsymbol{E}_{\text{ext}} = \boldsymbol{E}_0 + \frac{R^2}{\rho^2}D(\theta)\boldsymbol{E}_{\text{dip}} \tag{10}$$

Ann. Geophys. Discuss., https://doi.org/10.5194/angeo-2018-13
Manuscript under review for journal Ann. Geophys.
Discussion started: 13 February 2018

Annales Geophysicae Discussions Open Access

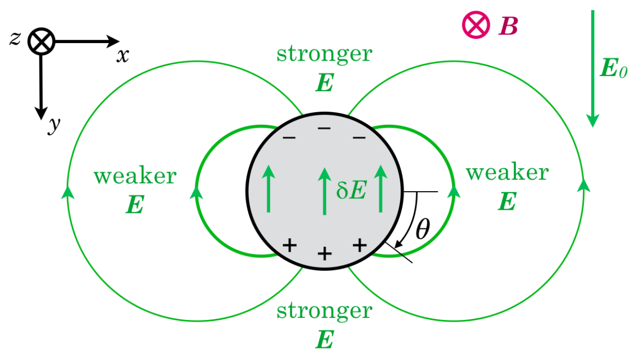

Figure 2. A circular patch of denser plasma will acquire a polarisation that reduces the electric field strength inside compared to the background field strength. This sets up a cylindrical (2-D) dipole. The $+$ and $-$ show net surface charge. The sense of the angle θ used in later analysis is also shown (the conventional sense, but appearing clockwise because $\hat{\boldsymbol{z}}$ is into the page). This figure ignores Hall current, but it is included in our analysis. The sense of plasma drift around such a feature is sketched in Fig. 3.

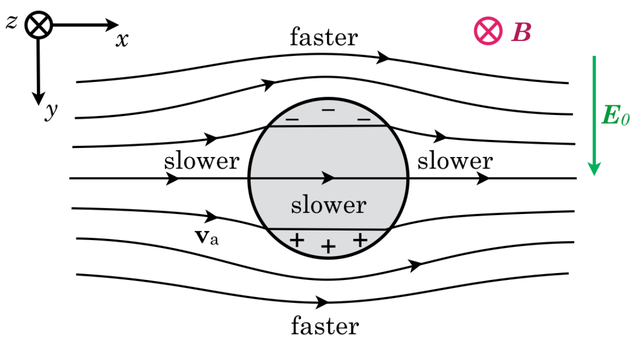

Figure 3. The polarisation of the patch in Fig. 2 establishes a dipole disturbance in the $\boldsymbol{E} \times \boldsymbol{B}$ drift. Note that plasma flows through the patch: while the density enhancement should retain its circular shape, the constituent ions are transient.

where R is the radius of the patch and D is a matrix defined in App. A.

When we take account of the Hall conductivity, we find that the dipole is no longer oriented exactly in the +y direction. Nor can $\boldsymbol{E}$ and $\boldsymbol{J}$ inside the patch be simply parallel, but scaled-down versions of their values outside the patch as they are for the slab, because the Hall current would then accumulate on the interface as a dipole oriented towards −x. The angle which $\boldsymbol{J}$ makes with $\boldsymbol{E}$ means that the positive pole of the dipole will be shifted from 6 o'clock in that figure toward 7 o'clock. So the field inside the patch, $\boldsymbol{E}_{\mathrm{int}}$, will be oriented somewhat towards 5 o'clock. If we assume a dipole orientation angle as a variable we can solve for both it and the dipole strength by requiring the current density expressions on the inner and outer sides of the circular boundary to be identical. (It is something like getting a doughnut and its hole to travel at the same speed.) Using the two mentioned parameters, this condition can be satisfied.

With $\boldsymbol{E}_0 = E_0\hat{\boldsymbol{y}}$ we assume the perimeter of the patch develops a surface charge density in the form of a rotated dipole:

$$\sigma_{\text{net}} = \sigma_x \cos\theta + \sigma_y \sin\theta \tag{11}$$

We solve for σ_x and σ_y under the condition that the current $\boldsymbol{J}$ into the boundary from the inside must balance the current on the outside. The outward normal is $\hat{\boldsymbol{n}} = [\cos\theta, \sin\theta]^T$.

3.1 Steady state currents around a circular, E-region patch

Using the result of App. A and the definition in Eq. (9), $\delta\boldsymbol{E}_{\text{int}} = -\boldsymbol{E}_{\text{dip}}$. For sake of brevity we let $\boldsymbol{k} = \boldsymbol{E}_{\text{dip}}$ for the coming passage up to Eq. (20).

$$\boldsymbol{J}_{\text{int}} = [\sigma]' \begin{bmatrix} -k_x \\ E_0 - k_y \end{bmatrix} \tag{12}$$

The current into the inner side of the boundary is

$$\begin{aligned} J_{\text{int}} &= \begin{bmatrix} -k_x\sigma_{\text{P}} - E_0\sigma_{\text{H}} + k_y\sigma_{\text{H}} \\ -k_x\sigma_{\text{H}} + E_0\sigma_{\text{P}} - k_y\sigma_{\text{P}} \end{bmatrix}' \cdot \hat{\boldsymbol{n}} \\ &= \cos\theta(-k_x\sigma_{\text{P}} - E_0\sigma_{\text{H}} + k_y\sigma_{\text{H}})' \\ &\quad + \sin\theta(-k_x\sigma_{\text{H}} + E_0\sigma_{\text{P}} - k_y\sigma_{\text{P}})' \end{aligned} \tag{13}$$

Using another result of App. A, at $\rho = R$,

$$\delta\boldsymbol{E}_{\text{ext}} = (k_x\cos\theta + k_y\sin\theta)\hat{\boldsymbol{\rho}} + (k_x\sin\theta - k_y\cos\theta)\hat{\boldsymbol{\theta}} \tag{14}$$

$$\boldsymbol{J}_{\text{ext}} = [\sigma] \begin{bmatrix} k_x\cos^2\theta + 2k_y\sin\theta\cos\theta - k_x\sin^2\theta \\ E_0 + 2k_x\sin\theta\cos\theta + k_y\sin^2\theta - k_y\cos^2\theta \end{bmatrix} \tag{15}$$

which after some straightforward steps yields a current *out of* the boundary of

$$\begin{aligned} J_{\text{ext}} &= E_0(\sigma_{\text{P}}\sin\theta - \sigma_{\text{H}}\cos\theta) + k_x\sigma_{\text{P}}\cos\theta \\ &\quad - k_x\sigma_{\text{H}}\sin\theta + k_y\sigma_{\text{P}}\sin\theta + k_y\sigma_{\text{H}}\cos\theta \end{aligned} \tag{16}$$

Setting the cosine terms in J_{int} and J_{ext} equal,

$$(\sigma_{\text{P}} + \sigma'_{\text{P}})k_x + (\sigma_{\text{H}} - \sigma'_{\text{H}})k_y = E_0(\sigma_{\text{H}} - \sigma'_{\text{H}}) \tag{17}$$

and setting the sine terms equal,

$$(-\sigma_{\text{H}} + \sigma'_{\text{H}})k_x + (\sigma_{\text{P}} + \sigma'_{\text{P}})k_y = E_0(-\sigma_{\text{P}} + \sigma'_{\text{P}}) \tag{18}$$

These two linear equations in k_x and k_y are

$$\begin{bmatrix} \sigma_\mathrm{P}+\sigma'_\mathrm{P} & \sigma_\mathrm{H}-\sigma'_\mathrm{H} \\ -\sigma_\mathrm{H}+\sigma'_\mathrm{H} & \sigma_\mathrm{P}+\sigma'_\mathrm{P} \end{bmatrix} \begin{bmatrix} k_x \\ k_y \end{bmatrix} = E_0 \begin{bmatrix} \sigma_\mathrm{H}-\sigma'_\mathrm{H} \\ -\sigma_\mathrm{P}+\sigma'_\mathrm{P} \end{bmatrix} \tag{19}$$

$$\Big[[\sigma]' + [\sigma]^T\Big] \begin{bmatrix} k_x \\ k_y \end{bmatrix} = \Big[[\sigma]' - [\sigma]\Big] \begin{bmatrix} 0 \\ E_0 \end{bmatrix} \tag{20}$$

The LHS represents the rate of loss of net charge from the dipole $\sigma = 2\varepsilon_0 E_\mathrm{dip}$. On the RHS, the *difference* in $[\sigma]$ between the patch and its surroundings is forcing its polarisation. Hence we can write

$$S\boldsymbol{E}_\mathrm{dip} = (n-1)[\sigma]\boldsymbol{E}_0 \tag{21}$$

where the matrix on the LHS is

$$S = \begin{bmatrix} \sigma_\mathrm{P}(n+1) & \sigma_\mathrm{H}(-n+1) \\ \sigma_\mathrm{H}(n-1) & \sigma_\mathrm{P}(n+1) \end{bmatrix} \tag{22}$$

which is *nearly* scalar for $n \approx 1$, but let us define H by writing

$$S = (n+1)\sigma_\mathrm{P} \begin{bmatrix} 1 & -\eta\sigma_\mathrm{H}/\sigma_\mathrm{P} \\ \eta\sigma_\mathrm{H}/\sigma_\mathrm{P} & 1 \end{bmatrix} = (n+1)\sigma_\mathrm{P} H \tag{23}$$

$$(n+1)\sigma_\mathrm{P} H \boldsymbol{E}_\mathrm{dip} = (n-1)[\sigma]\boldsymbol{E}_0 \tag{24}$$

Solving for $\boldsymbol{E}_\mathrm{dip}$, a polarisation with

$$\boldsymbol{E}_\mathrm{dip} = \frac{\eta}{\sigma_\mathrm{P}} H^{-1}[\sigma]\boldsymbol{E}_0 \tag{25}$$

yields a divergence-free current field.

The steady-state electric field in and around the patch, using Eqs. (A7) and (A8), is

$$\boldsymbol{E}_\mathrm{int} = \left(I - \frac{\eta}{\sigma_\mathrm{P}} H^{-1}[\sigma] \right) \boldsymbol{E}_0 \tag{26}$$

$$\boldsymbol{E}_\mathrm{ext} = \left(I + \frac{\eta R^2}{\sigma_\mathrm{P}\rho^2} D(\theta) H^{-1}[\sigma] \right) \boldsymbol{E}_0 \tag{27}$$

From this expression for $\boldsymbol{E}_\mathrm{int}$, one can verify that it is at an angle relative to $\boldsymbol{E}_0$ whose tangent is $\eta\sigma_\mathrm{H}/\sigma_\mathrm{P}$. This agrees with Hysell and Drexler's Eq. (9), which gives us confidence in our results, although we focus below on the *boundary*'s drift, rather than that of the ions inside.

Ann. Geophys. Discuss., https://doi.org/10.5194/angeo-2018-13
Manuscript under review for journal Ann. Geophys.
Discussion started: 13 February 2018

3.2 Simplifying assumptions

We shall deal here with a single ion species, and assume that electrons are fully magnetised. These assumptions are not necessary for a unique solution, but will greatly simplify the algebra. Under these assumptions, and using the ion magnetisation parameter $\kappa_\mathrm{i} = \omega_\mathrm{i}/\nu_\mathrm{in}$, we have

$$\sigma_\mathrm{P} = \frac{q_i n_i}{B}\left(\frac{\kappa_\mathrm{i}}{1+\kappa_\mathrm{i}^2}\right) \tag{28}$$

$$\sigma_\mathrm{H} = \frac{q_i n_i}{B}\left(\frac{1}{1+\kappa_\mathrm{i}^2}\right) \tag{29}$$

Thus $\sigma_\mathrm{P} = \kappa_\mathrm{i}\sigma_\mathrm{H}$, and $|\kappa_\mathrm{e}|$ is much larger than both κ_i and unity.

We also assume no neutral drift, or equivalently that the electric field and all of the species' drifts are expressed in the neutrals' frame of reference.

3.3 Species drift

The drift of a species s (ion or electron) in the plane perpendicular to $\boldsymbol{B}$ can be described by

$$\mathbf{v}_s = \begin{bmatrix} \mu_\mathrm{P} & \mu_\mathrm{a} \\ -\mu_\mathrm{a} & \mu_\mathrm{P} \end{bmatrix}_s \boldsymbol{E} \tag{30}$$

where

$$\mu_\mathrm{a} = \frac{\kappa_s^2}{B(1+\kappa_s^2)} \text{ and } \mu_\mathrm{P} = \frac{\kappa_s}{B(1+\kappa_s^2)} \tag{31}$$

are the ambipolar and Pedersen mobilities, respectively. If we let ϕ_s be an angle defined by $\kappa_s = \cot(\phi_s)$ then we can write the mobility matrix as

$$\begin{aligned}
\mathbf{v}_s &= \frac{1}{B}\begin{bmatrix} \sin\phi\cos\phi & \cos^2\phi \\ -\cos^2\phi & \sin\phi\cos\phi \end{bmatrix}_s \boldsymbol{E} \\
&= \frac{\cos\phi_s}{B}\begin{bmatrix} \sin\phi & \cos\phi \\ -\cos\phi & \sin\phi \end{bmatrix}_s \boldsymbol{E} \\
&= \frac{\cos\phi_s}{B} R(\phi_s - \tfrac{\pi}{2})\boldsymbol{E}
\end{aligned} \tag{32}$$

where R is a rotation matrix, anticlockwise if looking from positive z. We use R_s below as shorthand for $R(\phi_s - \frac{\pi}{2})$. Alternately, since $\mathbf{v}_\mathrm{a} = B^{-1}R(-\frac{\pi}{2})\boldsymbol{E}$,

$$\begin{aligned}
\mathbf{v}_s &= \cos\phi_s \begin{bmatrix} \cos\phi & -\sin\phi \\ \sin\phi & \cos\phi \end{bmatrix}_s \mathbf{v}_\mathrm{a} \\
&= \cos\phi_s R(\phi_s)\mathbf{v}_\mathrm{a}
\end{aligned} \tag{33}$$

where $\mathbf{v}_\mathrm{a}$ is the ambipolar drift. We see that ϕ_s is the angle which the species' drift makes w.r.t. the ambipolar drift, however we shall use the previous expression in order to get $\mathbf{v}_s$ as a function of $\boldsymbol{E}$.

3.4 Patch drift speed

Applying Eq. (4) to our dipole field,

$$\begin{aligned}\hat{\boldsymbol{n}}\cdot\mathbf{v}_\mathrm{b} &= \frac{\cos\phi_s}{(n-1)B}\,\hat{\boldsymbol{n}}\cdot(nR_s\boldsymbol{E}_\mathrm{int}-R_s\boldsymbol{E}_\mathrm{ext})\\ &= \frac{\cos\phi_s}{(n-1)B}\,\hat{\boldsymbol{n}}\cdot R_s\left[n\left(I-\frac{\eta}{\sigma_\mathrm{P}}H^{-1}[\sigma]\right)-\left(I+\frac{\eta}{\sigma_\mathrm{P}}DH^{-1}[\sigma]\right)\right]\boldsymbol{E}_0\\ &= \frac{\cos\phi_s}{(n-1)B}\,\hat{\boldsymbol{n}}\cdot R_s\left[(n-1)I-\frac{\eta}{\sigma_\mathrm{P}}(nI+D)H^{-1}[\sigma]\right]\boldsymbol{E}_0\end{aligned}\tag{34}$$

We now make use of Eq. (A11), the fact that $\hat{\boldsymbol{n}}^TR_sD=\hat{\boldsymbol{n}}^TR_s^T$. It can also be shown that

$$nR_s+R_s^T=(n+1)\sin\phi_s\begin{bmatrix}1 & \eta\kappa_s\\ -\eta\kappa_s & 1\end{bmatrix}\tag{35}$$

Let us call that last matrix M_s. Simplifying,

$$\hat{\boldsymbol{n}}\cdot\mathbf{v}_\mathrm{b}=\hat{\boldsymbol{n}}\cdot\left[\frac{\cos\phi_s}{B}R_s\boldsymbol{E}_0-\frac{\sin\phi_s\cos\phi_s}{B\sigma_\mathrm{P}}M_sH^{-1}[\sigma]\boldsymbol{E}_0\right]\tag{36}$$

The factor in square brackets on the RHS of the last equation has no θ dependence, and the tangential component of $\mathbf{v}_\mathrm{b}$ is arbitrary. So we may drop the $\hat{\boldsymbol{n}}$ from both sides and choose

$$\begin{aligned}\mathbf{v}_\mathrm{b} &= \frac{\cos\phi_s}{B}R_s\boldsymbol{E}_0-\frac{\sin\phi_s\cos\phi_s}{B\sigma_\mathrm{P}}M_sH^{-1}[\sigma]\boldsymbol{E}_0\\ &= \mathbf{v}_{s,0}-\frac{\sin\phi_s\cos\phi_s}{B\sigma_\mathrm{P}}M_sH^{-1}\boldsymbol{J}_0\end{aligned}\tag{37}$$

where the first term on the RHS is the background drift of the species, and we have used $\boldsymbol{J}=[\sigma]\boldsymbol{E}$. We now use $\boldsymbol{J}=q_\mathrm{i}n_\mathrm{i}(\mathbf{v}_\mathrm{i}-\mathbf{v}_\mathrm{e})$; $\sigma_\mathrm{P}=q_\mathrm{i}n_\mathrm{i}\kappa_\mathrm{i}/B(1+\kappa_\mathrm{i}^2)$; and $\kappa_\mathrm{i}=\cot\phi_\mathrm{i}$ to get (dropping the subscript 0 now since all quantities except η are background values)

$$\begin{aligned}\mathbf{v}_\mathrm{b} &= \mathbf{v}_s-\frac{\sin\phi_s\cos\phi_s}{\sin\phi_\mathrm{i}\cos\phi_\mathrm{i}}M_sH^{-1}(\mathbf{v}_\mathrm{i}-\mathbf{v}_\mathrm{e})\\ &= \mathbf{v}_s+\frac{\sin\phi_s\cos\phi_s}{\sin\phi_\mathrm{i}\cos\phi_\mathrm{i}}\begin{bmatrix}1 & \eta\kappa_s\\ -\eta\kappa_s & 1\end{bmatrix}\begin{bmatrix}1 & -\eta/\kappa_\mathrm{i}\\ \eta/\kappa_\mathrm{i} & 1\end{bmatrix}^{-1}(\mathbf{v}_\mathrm{e}-\mathbf{v}_\mathrm{i})\\ &= \mathbf{v}_s+\frac{\sin\phi_s\cos\phi_s}{\sin\phi_\mathrm{i}\cos\phi_\mathrm{i}}\begin{bmatrix}1 & \eta\kappa_s\\ -\eta\kappa_s & 1\end{bmatrix}\frac{\kappa_\mathrm{i}}{\kappa_\mathrm{i}^2+\eta^2}\begin{bmatrix}\kappa_\mathrm{i} & \eta\\ -\eta & \kappa_\mathrm{i}\end{bmatrix}(\mathbf{v}_\mathrm{e}-\mathbf{v}_\mathrm{i})\\ &= \mathbf{v}_s+\frac{\sin\phi_s\cos\phi_s}{\sin^2\phi_\mathrm{i}(\kappa_\mathrm{i}^2+\eta^2)}\begin{bmatrix}1 & \eta\kappa_s\\ -\eta\kappa_s & 1\end{bmatrix}\begin{bmatrix}\kappa_\mathrm{i} & \eta\\ -\eta & \kappa_\mathrm{i}\end{bmatrix}(\mathbf{v}_\mathrm{e}-\mathbf{v}_\mathrm{i})\end{aligned}\tag{38}$$

Ann. Geophys. Discuss., https://doi.org/10.5194/angeo-2018-13
Manuscript under review for journal Ann. Geophys.
Discussion started: 13 February 2018

This equation ought to yield the same answer for either ions or electrons. We first demonstrate this for $|\eta| \ll 1$.

For ions ($s = \mathrm{i}$) we obtain

$$\begin{aligned}\mathbf{v}_\mathrm{b} &= \mathbf{v}_\mathrm{i} + \frac{\cot\phi_\mathrm{i}}{\kappa_\mathrm{i}^2+\eta^2}\begin{bmatrix}\kappa_\mathrm{i}(1-\eta^2) & \eta(\kappa_\mathrm{i}^2+1)\\ -\eta(\kappa_\mathrm{i}^2+1) & \kappa_\mathrm{i}(1-\eta^2)\end{bmatrix}(\mathbf{v}_\mathrm{e}-\mathbf{v}_\mathrm{i})\\ &= \mathbf{v}_\mathrm{i} + \begin{bmatrix}1 & \eta(\kappa_\mathrm{i}^2+1)/\kappa_\mathrm{i}\\ -\eta(\kappa_\mathrm{i}^2+1)/\kappa_\mathrm{i} & 1\end{bmatrix}(\mathbf{v}_\mathrm{e}-\mathbf{v}_\mathrm{i}) + O(\eta^2)\end{aligned} \tag{39}$$

The matrix is approximately a rotation, anticlockwise if we are looking parallel to $\boldsymbol{B}$, by a small angle

$$\begin{aligned}\alpha &\approx \frac{\eta(\kappa_\mathrm{i}^2+1)}{\kappa_\mathrm{i}}\\ &= \frac{(n-1)\csc^2\phi_\mathrm{i}}{(n+1)\cot\phi_\mathrm{i}}\\ &\approx \frac{(n-1)}{\sin 2\phi_\mathrm{i}}\end{aligned} \tag{40}$$

where in the last step we use $n+1 \approx 2$. See Fig. 4 for a sketch of this construction of $\mathbf{v}_\mathrm{b}$.

For electrons ($s = \mathrm{e}$) we obtain, using $\kappa_\mathrm{e} \ll -1$

$$\begin{aligned}\mathbf{v}_\mathrm{b} &= \mathbf{v}_\mathrm{e} + \frac{\sin\phi_\mathrm{e}\cos\phi_\mathrm{e}}{\sin^2\phi_\mathrm{i}(\kappa_\mathrm{i}^2+\eta^2)}\begin{bmatrix}1 & \eta\kappa_\mathrm{e}\\ -\eta\kappa_\mathrm{e} & 1\end{bmatrix}\begin{bmatrix}\kappa_\mathrm{i} & \eta\\ -\eta & \kappa_\mathrm{i}\end{bmatrix}(\mathbf{v}_\mathrm{e}-\mathbf{v}_\mathrm{i})\\ &= \mathbf{v}_\mathrm{e} + \frac{\sin\phi_\mathrm{e}\cos\phi_\mathrm{e}}{\sin^2\phi_\mathrm{i}\cot^2\phi_\mathrm{i}}\eta\kappa_\mathrm{e}\begin{bmatrix}0 & 1\\ -1 & 0\end{bmatrix}\kappa_\mathrm{i}\begin{bmatrix}1 & 0\\ 0 & 1\end{bmatrix}(\mathbf{v}_\mathrm{e}-\mathbf{v}_\mathrm{i}) + O(\eta^2)\\ &= \mathbf{v}_\mathrm{e} + \eta\frac{\cos^2\phi_\mathrm{e}}{\sin\phi_\mathrm{i}\cos\phi_\mathrm{i}}R(-\tfrac{\pi}{2})(\mathbf{v}_\mathrm{e}-\mathbf{v}_\mathrm{i})\\ &= \mathbf{v}_\mathrm{e} + \frac{(n-1)}{\sin 2\phi_\mathrm{i}}R(-\tfrac{\pi}{2})(\mathbf{v}_\mathrm{e}-\mathbf{v}_\mathrm{i}) + O(\kappa_\mathrm{e}^{-1})\end{aligned} \tag{41}$$

Fig. 4 also sketches this construction of $\mathbf{v}_\mathrm{b}$, and one can see it is coïncident with the value of $\mathbf{v}_\mathrm{b}$ obtained using the ions.

The magnitude of this drift, relative to the electron ($\approx$ ambipolar) drift is

$$\begin{aligned}\mathrm{v}_\mathrm{b} &= \frac{(n-1)}{\sin 2\phi_\mathrm{i}}|\mathbf{v}_\mathrm{e}-\mathbf{v}_\mathrm{i}|\\ &= \frac{(n-1)}{\sin 2\phi_\mathrm{i}}\sin\phi_\mathrm{i}\mathrm{v}_\mathrm{a}\\ &\approx \tfrac{1}{2}(n-1)\sec\phi_\mathrm{i}\mathrm{v}_\mathrm{a}\end{aligned} \tag{42}$$

and the orientation of the patch's drift is at right angles to $\boldsymbol{J}_0$. It is slower than v_a for the case of density enhancements and faster for density depletions. Curiously, the drift of an enhancement's boundary has a component *against* the electric field.

Ann. Geophys. Discuss., https://doi.org/10.5194/angeo-2018-13
Manuscript under review for journal Ann. Geophys.
Discussion started: 13 February 2018

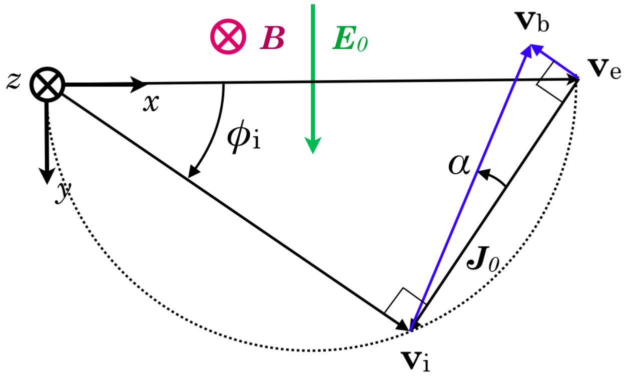

Figure 4. The dashed semicircle shows the locus of $\mathbf{v}_\mathrm{i}$ for various values of κ_i. The blue arrows show the construction of $\mathbf{v}_\mathrm{b}$, the drift of the density enhancement, relative to either the ion or electron background drift, for a modest enhancement ($n \gtrsim 1$).

3.5 General solution for arbitrary relative density

Still restricting ourselves to the three simplifying assumptions (one ion species, magnetised electrons, no neutral drift) we can determine the drift velocity of a patch or depletion with n much smaller or larger than unity.

Using Eq. (38), with either species, we can show that in the limit of large n, $\mathbf{v}_\mathrm{b} \to 0$. In the limit of $n \to 0$ (a deep hole), we get $\mathbf{v}_\mathrm{b} \to 2\mathbf{v}_\mathrm{i}$. And of course for $n = 1$ we have $\mathbf{v}_\mathrm{b} = \mathbf{v}_\mathrm{a}$. Looking at the trend for $n \sim 1$ suggested by Fig. 4, and using the intuition obtained with a bit of numerical experimentation, one can appreciate that the range of values which $\mathbf{v}_\mathrm{b}$ can take on as a function of n, for a fixed value of κ_i, describes a circular arc passing through the origin, $\mathbf{v}_\mathrm{a}$ and $2\mathbf{v}_\mathrm{i}$.

Since the origin and $\mathbf{v}_\mathrm{a}$ both lie on the circular arc, the arc's centre must lie on the line $\mathrm{v}_x = \frac{1}{2}\mathrm{v}_\mathrm{a}$. Furthermore, the trend around $n \sim 1$ being perpendicular to $\boldsymbol{J}$ shows that the centre lies along the line of $\boldsymbol{J}$ extended from $\mathbf{v}_\mathrm{a}$. Thus the centre is at $\mathbf{v}_\mathrm{cent} = \frac{1}{2}\mathrm{v}_\mathrm{a}[1, \cot\phi_\mathrm{i}]^T$. So we can separate the centre from the rest of Eq. (38) and, using $s = \mathrm{e}$ and repeating the same $O(\kappa_\mathrm{e}^{-1})$

Ann. Geophys. Discuss., https://doi.org/10.5194/angeo-2018-13
Manuscript under review for journal Ann. Geophys.
Discussion started: 13 February 2018

approximations used to get Eq. (41), write

$$
\begin{aligned}
\mathbf{v}_\mathrm{b} &= \mathbf{v}_\mathrm{cent} - \tfrac{1}{2}\begin{bmatrix} 1 \\ \cot\phi_\mathrm{i} \end{bmatrix} \mathrm{v}_\mathrm{a} + \mathbf{v}_\mathrm{e} + \frac{\eta}{\sin^2\phi_\mathrm{i}(\kappa_\mathrm{i}^2+\eta^2)} \begin{bmatrix} -\eta & \kappa_\mathrm{i} \\ -\kappa_\mathrm{i} & -\eta \end{bmatrix} (\mathbf{v}_\mathrm{e} - \mathbf{v}_\mathrm{i}) \\
&= \mathbf{v}_\mathrm{cent} + \tfrac{1}{2}\begin{bmatrix} 1 \\ -\cot\phi_\mathrm{i} \end{bmatrix} \mathrm{v}_\mathrm{a} + \frac{\csc^2\phi_\mathrm{i}\eta}{(\kappa_\mathrm{i}^2+\eta^2)} \begin{bmatrix} -\eta & \kappa_\mathrm{i} \\ -\kappa_\mathrm{i} & -\eta \end{bmatrix} \sin\phi_\mathrm{i} \begin{bmatrix} \sin\phi_\mathrm{i} \\ -\cos\phi_\mathrm{i} \end{bmatrix} \mathrm{v}_\mathrm{a} \\
&= \mathbf{v}_\mathrm{cent} + \tfrac{1}{2}\csc\phi_\mathrm{i} R(\phi_\mathrm{i} - \tfrac{\pi}{2}) \begin{bmatrix} 1 \\ 0 \end{bmatrix} \mathrm{v}_\mathrm{a} + \frac{\csc\phi_\mathrm{i}\eta}{(\kappa_\mathrm{i}^2+\eta^2)} \begin{bmatrix} -\eta & \kappa_\mathrm{i} \\ -\kappa_\mathrm{i} & -\eta \end{bmatrix} R(\phi_\mathrm{i} - \tfrac{\pi}{2}) \begin{bmatrix} 1 \\ 0 \end{bmatrix} \mathrm{v}_\mathrm{a} \\
&= \mathbf{v}_\mathrm{cent} + \frac{\csc\phi_\mathrm{i}}{2(\kappa_\mathrm{i}^2+\eta^2)} R(\phi_\mathrm{i} - \tfrac{\pi}{2}) \left((\kappa_\mathrm{i}^2+\eta^2) \begin{bmatrix} 1 \\ 0 \end{bmatrix} + 2\eta \begin{bmatrix} -\eta \\ -\kappa_\mathrm{i} \end{bmatrix} \right) \mathrm{v}_\mathrm{a} \\
&= \mathbf{v}_\mathrm{cent} + \frac{\csc\phi_\mathrm{i}}{2(\kappa_\mathrm{i}^2+\eta^2)} R(\phi_\mathrm{i} - \tfrac{\pi}{2}) \begin{bmatrix} \kappa_\mathrm{i}^2 - \eta^2 \\ -2\kappa_\mathrm{i}\eta \end{bmatrix} \mathrm{v}_\mathrm{a}
\end{aligned}
\tag{43}
$$

Let β be an angle defined by $\tan\beta = \eta/\kappa_\mathrm{i}$ (this is the angle between $\boldsymbol{E}_\mathrm{int}$ and $\boldsymbol{E}_0$). Then

$$
\begin{aligned}
\mathbf{v}_\mathrm{b} &= \mathbf{v}_\mathrm{cent} + \frac{\csc\phi_\mathrm{i}}{2(1+\tan^2\beta)} R(\phi_\mathrm{i} - \tfrac{\pi}{2}) \begin{bmatrix} 1-\tan^2\beta \\ -2\tan\beta \end{bmatrix} \mathrm{v}_\mathrm{a} \\
&= \mathbf{v}_\mathrm{cent} + \tfrac{1}{2}\csc\phi_\mathrm{i} R(\phi_\mathrm{i} - \tfrac{\pi}{2}) \begin{bmatrix} \cos 2\beta \\ \sin 2\beta \end{bmatrix} \mathrm{v}_\mathrm{a} \\
&= \mathbf{v}_\mathrm{cent} + \tfrac{1}{2}\csc\phi_\mathrm{i} R(\phi_\mathrm{i} - 2\beta - \tfrac{\pi}{2}) \mathbf{v}_\mathrm{a}
\end{aligned}
\tag{44}
$$

Fig. 5 illustrates the portion of the arc along which the boundary drift $\mathbf{v}_\mathrm{b}$ can occur for various density ratios n, for one particular value of κ_i.

If we look at the electron drift velocity inside the patch using Eqs. (26) and (32), we find that the electrons drift along with the boundary. So the patch (or depletion) keeps its original electrons (so to speak) whereas the ions are transiently within it, as in the slab geometry.

In Fig. 6 we show a series of possibilities for different ion magnetisation ratios from 0.1 to 10. Each coloured arc shows, for a fixed value of κ_i, how patches or depletions (varying n, or η) should drift. An enhancement always drifts slower than ambipolar, with a component against $\boldsymbol{E}$, whereas a depletion always has a component parallel to $\boldsymbol{E}$. Usually a depletion drifts faster than ambipolar, but with highly demagnetised ions an enhancement's drift can be slower.

In the frame of reference of the background drift, the current vector $\boldsymbol{J}$ separates the two cases, with enhancements drifting towards its right side (boreal pole), and depletions towards its left.

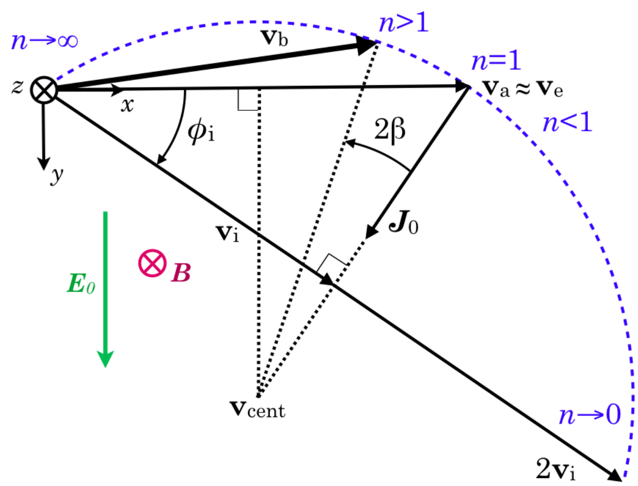

Figure 5. The construction of the circular arc (blue dotted curve) along which the drift of the boundary of a circular patch ($\mathbf{v}_\mathrm{b}$) can occur for a given ion magnetisation κ_i. The blue text shows the variation of the drift along the arc for various values of the relative density n, which determines the angle β. In this example $\kappa_\mathrm{i} \sim 1.5$.

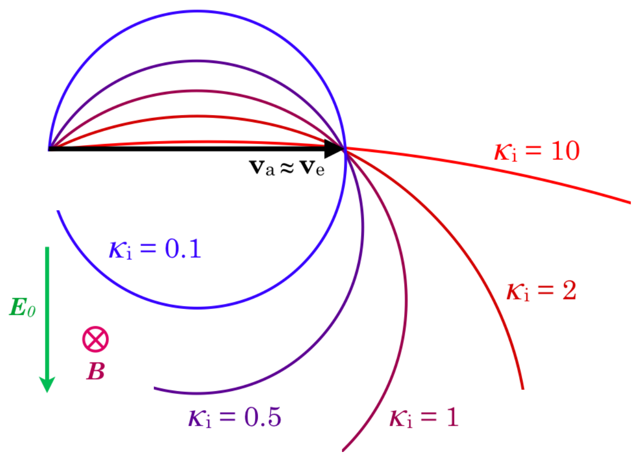

Figure 6. The variation w.r.t. ion magnetisation κ_i of the arc along which the drift of a circular patch can lie. All of the arcs coïncide at the origin (the limit of high n) and at the ambipolar drift (for the case of $n = 1$). An enhancement always drifts slower than ambipolar, with a component against $\boldsymbol{E}$, whereas a depletion always has a component parallel to $\boldsymbol{E}$.

4 Discussion

We have derived the drift behaviour of a circular density enhancement (or depletion) in a 2-D magnetised plasma. Our study grew from a 2-D auroral modeling effort in the *meridional* plane (de Boer et al., 2010) which led to thinking about appropriate upper boundary conditions (~ 1000 km) for the electric potential, and the time scales over which various effects should assert themselves. The eventual conclusion was that $J_{\parallel}=0$ was appropriate over the time scales of interest, and this inquiry led to the arguments presented above in justifying the 2-D analysis in a surface *perpendicular to* $\boldsymbol{B}$.

The idea that charge accumulation from a non-uniform conductivity $[\sigma]$ would set up an electric field disturbance in a way that would force the system towards steady-state ($\nabla \cdot \boldsymbol{J} = 0$) is simple, although the algebra turned out to be more complicated than expected. Perhaps a shorter derivation is possible. But we found a unique result that we are confident in.

Still, one might challenge the relevance of our result in the limit as $\kappa_{\mathrm{i}} \to \infty$, since the time required to approach an equilibrium condition also tends to infinity. However by following other lines of argument not included in this paper, and considering the effective, perpendicular *permittivity* of a magnetised plasma with $\kappa_{\mathrm{i}} \to \infty$, it can be shown that the steady-state towards which the E-region is driving the convection pattern is the same as the $\boldsymbol{E}_{\perp}$ structure obtained from considering a circular patch (or depletion) with $\boldsymbol{E}$ initially zero, and increasing $\boldsymbol{E}_0$ up to some steady value.

One should also reasonably question how these 2-D results – specifically Eq. (44) – can be extended to the real ionosphere, where κ_{i} and ϕ_{i} vary continuously with height. Each altitude layer will be forcing a different patch drift speed, while parallel conductivity is trying to enforce a coherent flux-tube drift. A conjecture (which awaits analytic justification) is that the *effective* ion magnetisation of a flux tube can be obtained from the ratio of height-integrated conductivities:

$$\kappa_{\text{eff.}} = \Sigma_P / \Sigma_H \tag{45}$$

and that values of ϕ_{i} and β determined from this $\kappa_{\text{eff.}}$ can be used in Eq. (44) to find the theoretical drift direction and speed of a patch (or a depletion). Of course such a 3-D drift structure would entail dipolar structures of FACs closed *within the ionosphere*. There would be a special height at which $\kappa_{\text{eff.}} = \kappa_{\mathrm{i}}$, and the dipolar FAC would be oppositely oriented above and below this height.

It may be possible to extend our analysis to elliptical patches. However it has some complexities that might only yield to complex analysis, as Hysell and Drexler (2006) have accomplished. At least this study reinforces their result for circular patches.

We have studied patches with sharp, step boundaries in density, which is an idealisation. The warm-plasma mechanism of ion diffusion, which operates on time and distance scales not addressed in this paper, would gradually degrade such a sharp step, as would any instabilities along the boundary, for example the shear-driven instability (SDI). However one can also see that any perturbation of the boundary, while suffering some SDI growth at the 12 and 6 o'clock positions in Fig. 3, will ultimately be convected towards the 3 o'clock position, where the shear approaches zero. This would prevent the growth of longer-wavelength (hence slower-growing) modes more than short-wavelength (faster-growing) ones. So SDI would also gradually blunt the sharpness of the boundary, but it does not necessarily imply the complete breakup of the patch as a distinct entity. We examine the sharp, circular case because it yields to analysis, and because we can make useful qualitative arguments based on the results.

Ann. Geophys. Discuss., https://doi.org/10.5194/angeo-2018-13
Manuscript under review for journal Ann. Geophys.
Discussion started: 13 February 2018

4.1 Implications for gradient scale lengths

It is impossible to extend these analytical methods to arbitrary shapes. But it seems clear that a patch with concentric contours of density would have a progressive drift, relative to ambipolar, that grows as one looks deeper within the patch. As a thought experiment, consider a small, denser patch within a larger patch. While an analytical result may be elusive except for the moment at which they are concentric, and neither will remain exactly circular, qualitatively we know that the inner patch will drift within the larger one, and that this relative drift will see it approach the outer boundary on the side opposite to $\mathbf{v}_\mathrm{i}$. (The curves in Fig. 6 are tangent to $\mathbf{v}_\mathrm{i}$ at $\mathbf{v}_\mathrm{a}$.)

Therefore we expect to see that any gradual density features would evolve in such a way that their gradients 'pile up' on one side and get stretched out on the other. In the case of banded structures, this may produce something like a saw-tooth density profile. If $\nabla_\perp \rho_\mathrm{m}$ is the gradient of plasma mass density ρ_m, then the steepest gradients should be found parallel to the *ion* drift (not the $\boldsymbol{E}\times\boldsymbol{B}$ drift), with $\nabla_\perp \rho_\mathrm{m}$ oriented in the same sense.

Such a steepening of mass density gradients would entail polarisations and electric field structures on the same scale lengths. Unless these are already uniform along magnetic field lines, FAC's will arise so that the plasma along any given flux tube accelerates to regain a coherent drift. One of the conclusions of de Boer et al. (2010) was that the ionosphere's response to precipitation could be FAC over a much *larger* region than the precipitation, and that FAC structure was a convolution of the precipitation structure, so that it always had larger gradient scale lengths. However in this paper we see the possibility of the ionosphere developing very short gradient scale lengths and generating FAC over equally small scales, *smaller than any initial density structure*, without the requirement for precipitation to initiate the fine-scale structure.

This effect could explain why in auroral phenomena we see structures cascading to smaller and smaller gradient scale lengths. The initial density gradients generated in the polar oval by precipitation are stronger to begin with than at other latitudes. Also the strong electric fields found there reduce the time scale for features to cascade to smaller spatial scales. This combination of conditions yields an increased chance that this cascade time scale might prevail over the erasure of structure on the scale of the ion chemical lifetime.

4.2 Search for observational support

The predicted structuring of the electric field around density features, and the relative drift of those features, is independent of scale. Hysell and Drexler were motivated by Farley-Buneman waves. We began with the goal of understanding small-scale auroral structure, however an observational test of our results for individual features would appear to be very difficult. The most promising avenue for testing our hypotheses will be in the observation of large-scale patches in the polar cap and oval. Both Carlson (2012) and Zhang et al. (2013) have provided analyses of events using, respectively, EISCAT for Ne data and GPS receiver arrays for TEC. The latter dataset is overlaid with SuperDARN convection patterns. These papers show incontrovertibly that patches of ionisation do cross the polar cap, and can return in the sunward return flow. However within the spatial and temporal resolution of their available data, it is challenging to see either confirmation or refutation of the electric-field structuring that we posit.

5 Conclusions

The following characteristics of $\boldsymbol{E} \times \boldsymbol{B}$ drift in 2-D, magnetised plasma, shown by Hysell and Drexler (2006), have been confirmed through an alternate analysis:

1. While plasma on an open flux tube may have a uniform electric field more-or-less "imposed" on it regardless of density structure, plasma on closed flux tubes will experience a structuring of the steady-state electric field that depends on density features – weighted towards dependence on E-region density.

2. For a circular density feature, the assumption of a dipolar net charge with appropriate magnitude and orientation can yield a divergence-free current field.

3. A density feature does not "own" a particular parcel of ions – the ions both inside and out can convect through the boundary – nevertheless the boundary of a circular density feature retains a circular shape, and the electrons convect with the density feature.

We have also shown that:

4. The boundary of a circular feature should convect with a velocity given by Eq. (44) and shown in Fig. 6 – always slower than ambipolar for an enhancement and usually faster for a depletion; and with a component against or with, respectively, the background electric field.

5. An obvious extension of the result for a sharp, circular feature is that features with density *gradients* will see gradients on one side steepened and gradients on the other side weakened.

6. The E-region can therefore generate smaller-scale structure than its initial structure, at any length scale and even without instability present, and the time scale for this to occur is inversely related to the electric field strength.

As well, we have provided some arguments as to why and how these 2-D results are still applicable to the real ionosphere with its altitude-dependence of plasma properties. Moreover, we wish to show in a future paper that the structuring described at point 1., in a *non-conducting* plasma, will depend on plasma *mass* density features.

Code availability. n/a

Data availability. n/a

Code and data availability. n/a

Appendix A: Cylindrical dipole

Let a circle of radius R have a surface charge density $\sigma = s\cos\theta$. The electric field inside is uniform: $\boldsymbol{E}_{\text{int}} = -a\hat{\boldsymbol{x}}$. Outside it has the form $E_\rho = b\rho^{-2}\cos\theta$ and $E_\theta = b\rho^{-2}\sin\theta$.

At the centre, using an expression for the electric field around an infinite line of charge and symmetry,

$$
\begin{aligned}
a = |\boldsymbol{E}_{\text{int}}| &= 2\int\limits_{-\pi/2}^{\pi/2} \frac{sR\cos\theta}{2\pi\varepsilon_0 R}\cos\theta\,\mathrm{d}\theta \\
&= \frac{2s}{2\pi\varepsilon_0}\cdot 2\int\limits_{0}^{\pi/2}\cos^2\theta\,\mathrm{d}\theta \\
&= \frac{2s}{\pi\varepsilon_0}\cdot\frac{\pi}{4} = \frac{s}{2\varepsilon_0}
\end{aligned}
\tag{A1}
$$

At the pole ($\theta = 0$), using Gauss' law,

$$\boldsymbol{E}_{\text{ext}} - \boldsymbol{E}_{\text{int}} = \frac{s}{\varepsilon_0}\hat{\boldsymbol{x}} \tag{A2}$$

$$bR^{-2} + \frac{s}{2\varepsilon_0} = \frac{s}{\varepsilon_0} \tag{A3}$$

$$b = \frac{sR^2}{2\varepsilon_0} = aR^2 \tag{A4}$$

The polarisation vector $\boldsymbol{P}$ inside the circle is $s\hat{\boldsymbol{x}}$. The field outside is

$$
\begin{aligned}
\boldsymbol{E}_{\text{ext}} &= \frac{b}{\rho^2}(\cos\theta\,\hat{\boldsymbol{\rho}} + \sin\theta\,\hat{\boldsymbol{\theta}}) \\
&= \frac{sR^2}{2\varepsilon_0\rho^2}\begin{bmatrix} 2\cos^2\theta - 1 \\ 2\sin\theta\cos\theta \end{bmatrix}
\end{aligned}
\tag{A5}
$$

If we generalise the charge dipole to an arbitrary orientation:

$$\sigma = s_x\cos\theta + s_y\sin\theta \tag{A6}$$

then we can express the cylindrical dipole field as

$$\boldsymbol{E}_{\text{int}} = \frac{-1}{2\varepsilon_0}\begin{bmatrix} s_x \\ s_y \end{bmatrix} \tag{A7}$$

$$\boldsymbol{E}_{\text{ext}} = \frac{R^2}{2\varepsilon_0\rho^2}D\begin{bmatrix} s_x \\ s_y \end{bmatrix} \tag{A8}$$

where we introduce a matrix $D(\theta)$ defined as

$$D = \begin{bmatrix} 2\cos^2\theta - 1 & 2\sin\theta\cos\theta \\ 2\sin\theta\cos\theta & 2\sin^2\theta - 1 \end{bmatrix}$$
$$= \begin{bmatrix} \cos 2\theta & \sin 2\theta \\ \sin 2\theta & -\cos 2\theta \end{bmatrix} \tag{A9}$$

D has the following property: Let A be any matrix of the form

$$A = \begin{bmatrix} a & -b \\ b & a \end{bmatrix} \tag{A10}$$

(Such a matrix combines a rotation with an isotropic scaling.) If $\hat{\boldsymbol{n}}$ (or $\hat{\boldsymbol{\rho}}$) is an outward unit vector $[\cos\theta, \sin\theta]^T$, then

$$\hat{\boldsymbol{n}}^T DA = \hat{\boldsymbol{n}}^T A, \text{ whereas } \hat{\boldsymbol{n}}^T AD = \hat{\boldsymbol{n}}^T A^T. \tag{A11}$$

Appendix B: Time dependence

We show in the main text that for a free-charge dipole σ_{free} oriented towards $\hat{\boldsymbol{k}}$,

$$\frac{\mathrm{d}}{\mathrm{d}t}\sigma_{\text{free}}\hat{\boldsymbol{k}} = -S\boldsymbol{E}_{\text{dip}} \tag{B1}$$

Now, $\sigma_{\text{net}}\hat{\boldsymbol{k}} = 2\varepsilon_0\boldsymbol{E}_{\text{dip}}$ and $\sigma_{\text{free}} = \chi_{\text{e}}\sigma_{\text{net}}$, so the homogeneous behaviour of $\boldsymbol{E}_{\text{dip}}$ is

$$\frac{\mathrm{d}}{\mathrm{d}t}\boldsymbol{E}_{\text{dip}} = \frac{-S}{2\chi_{\text{e}}\varepsilon_0}\boldsymbol{E}_{\text{dip}} \tag{B2}$$

The forcing term in Eq. (25) determines the steady-state value of $\boldsymbol{E}_{\text{dip}}$, but the characteristic time τ required to *settle* on that value depends only on the inverse of the coefficient of this homogeneous term.

The matrix S is of order σ_{P} and the effective, low-frequency, perpendicular susceptibility of a magnetised plasma is $\chi_{\text{e}} = \rho_{\text{m}}/\varepsilon_0 B^2$, where ρ_{m} is the plasma mass density. Hence

$$\tau \sim \frac{\chi_{\text{e}}\varepsilon_0}{\sigma_{\text{P}}} = \frac{(1+\kappa_{\text{i}}^2)}{\omega_{\text{i}}\kappa_{\text{i}}} = \frac{\csc\phi_{\text{i}}\sec\phi_{\text{i}}}{\omega_{\text{i}}} = \frac{\sec^2\phi_{\text{i}}}{\nu_{\text{in}}} \sim \frac{1}{\nu_{\text{in}}} \tag{B3}$$

So the time scale for the E-region alone to settle on a density-dependent drift speed is of the order of the mean time between ion-neutral collisions. The drift momentum of the F-region multiplies this by a further factor, equal to the ratio of F- to E-region integrated mass density, and this brings the time scale to the order of a second.

The magnetospheric contribution to total flux-tube drift momentum also delays the structuring of the electric field as its momentum is used up by ionospheric ion-neutral collisions. The magnetospheric contribution of momentum is significantly more than the F-region's, but it arrives only after a transport delay due to Alfvén propagation of order 5 minutes. So the much larger magnetospheric drift momentum, making itself felt over so long a time, does not slow the approach to steady state as intensely as the F-region does. And even this momentum does not change the *steady-state* drift velocity ($\boldsymbol{E}_\perp$ structure) of the patch or depletion, which on closed field lines is determined by the E-region conductivity differences alone.

Ann. Geophys. Discuss., https://doi.org/10.5194/angeo-2018-13
Manuscript under review for journal Ann. Geophys.
Discussion started: 13 February 2018

Annales Geophysicae
Discussions

Competing interests. None exist.

Acknowledgements. The authors would like to acknowledge helpful contributions from K. Kabin and P. Perron.

References

Baumjohann, W. and Treumann, R. A.: Basic Space Plasma Physics, Imperial College Press, London, 1996.

Carlson, H. C.: Sharpening our thinking about polar cap ionospheric patch morphology, research and mitigation techniques, Radio Science, 47, RSOL21, 2012.

de Boer, J. D., Noël, J.-M. A., and St.-Maurice, J.-P.: The effects of mesoscale regions of precipitation on the ionospheric dynamics, electrodynamics and electron density in the presence of strong ambient electric fields, Ann. Geophys., 28, 1345–1360, 2010.

Hysell, D. L. and Drexler, J.: Polarisation of elliptic E region plasma irregularities and implications for coherent radar backscatter from Farley-Buneman waves, Radio Science, 41, https://doi.org/10.1029/2005RS003424, 2006.

Mallinson, J. C.: On the Properties of Two-Dimensional Dipoles and Magnetized Bodies, IEEE Transactions on Magnetics, MAG-17, 2453–2460, 1981.

Zhang, Q.-H., Zhang, B.-C., Lockwood, M., Hu, H.-Q., Moen, J., Ruohoniemi, J. M., Thomas, E. G., Zhang, S.-R., Yang, H.-G., Liu, R.-Y., McWilliams, K. A., and Baker, J. B. H.: Direct Observations of the Evolution of Polar Cap Ionization Patches, Science, 339, 1597–1600, 2013.